Errata to AUTHORSHIP AND ACKNOWLEDGEMENTS IN "SPHERICAL SLOTTED ANTENNA COATED WITH DOUBLE LAYER OF MATERIALS HAVING COMBINATIONS OF SINGLY AND DOUBLY NEGATIVE PARAMETERS AND CONSEQUENCES OF MODE RESONANCES"
by M. Ng Mou Kehn, in *Progress In Electromagnetics Research B*, Vol. 45, pp. 223–249, 2012

M. Ng Mou Kehn

Department of Electrical and Computer Engineering
Institute of Communications Engineering
National Chiao Tung University
1001 University Road, Hsinchu 300, Taiwan

The author of the errata as well as the stated article "Spherical slotted antenna coated with double layer of materials having combinations of singly and doubly negative parameters and consequences of mode resonances" (appeared in PIERB, Vol. 45, 223–249, 2012) had negligently left out a coauthor. The correct list of authors for this paper should be, in this order:

L. Shafai* and M. Ng Mou Kehn**
* Department of Electrical and Computer Engineering
University of Manitoba, Canada
** Institute of Communications Engineering
National Chiao Tung University, Taiwan

Also, the acknowledgment was incorrectly stated. It should instead have read: "This work was supported by the Natural Sciences and Engineering Research Council (NSERC) of Canada and the Department of Electrical and Computer Engineering at the University of Manitoba, Canada."

It is only from recent events where the author has come to realize these errors, for which he deeply regrets. He hereby apologizes sincerely to his rightful coauthor Prof. L. Shafai as well as to NSERC and the University of Manitoba for the blunder.

Progress In Electromagnetics Research B, Vol. 45, 223–249, 2012

SPHERICAL SLOTTED ANTENNA COATED WITH DOUBLE LAYER OF MATERIALS HAVING COMBINATIONS OF SINGLY AND DOUBLY NEGATIVE PARAMETERS AND CONSEQUENCES OF MODE RESONANCES

M. Ng Mou Kehn*

Department of Electrical and Computer Engineering, Institute of Communications Engineering, National Chiao Tung University, 1001 University Road, Hsinchu 300, Taiwan

Abstract—This work studies the influence of material coatings, especially combined natural and metamaterials, on the radiation properties of a practical dipole like antenna, represented by a slotted conducting sphere. The selected geometry allows an exact solution to the problem, and thus the development of exact expressions for the antenna parameters, like the radiated power and directivity. It is shown that for materials with combined positive and negative parameters, mode resonances can occur at thinner coatings, the thickness of which can be made diminishingly small by proper selection of coating parameters. In particular, at these resonances the antenna directivity, while being finite, becomes independent of the antenna size and coating parameters.

1. INTRODUCTION

A conducting sphere represents a canonical problem in electromagnetics and is well investigated by many authors over the past few decades. Its specific geometry provides exact analytic solutions for a variety of problems involving spherical shapes and more complex related configurations like slotted and coated spheres [1–3]. The study of slots on perfectly conducting spheres and coated spheres can be traced as far back as over half a century ago. Karr [1] in 1951 investigated the effects of the electrical radius and the position of the slot on the radiation properties of a metallic uncoated sphere. A few years later,

Received 11 August 2012, Accepted 25 October 2012, Scheduled 30 October 2012

* Corresponding author: Malcolm Ng Mou Kehn (malcolmaxwell@gmail.com).

Mushiake and Webster [2] reported the radiation patterns, impedances, and power gains of nonsymmetrically excited narrow azimuthal slots on a sphere. The work by Kerker [3] has given a summarized description of the scattering from coated and stratified spheres. Shortly after, Towaij and Hamid [4] looked into the radiation characteristics of an azimuthal slot on a perfectly conducting sphere coated with multiple layers of dielectric materials. The case of slotted spheres includes both scattering and antenna problems, and in the latter case, enables analytic solutions for their impedance and radiation properties. However, up till that point in time, the effects of the coating thickness and other physical parameters on the radiated power had not yet been thoroughly investigated. An interesting problem involving coated spheres is the resonance phenomenon due to the coating, when one of the spherical modes becomes resonant. While such resonances manifest similar mathematical problems in scattering and antenna applications, they have fundamentally different implications in each. In the former case, it influences the scattering properties of the sphere, while in the latter it affects both the radiation as well as the input impedance parameters. Nonetheless, in both cases it enhances the contribution of resonant modes to the field quantities.

In the case of spherical antennas, the resonance phenomena in the coating were originally investigated by Shafai and Chugh [5] in 1973, which identified the resonant modes and studied their influences on the radiated power. An azimuthally slotted conducting spherical antenna was selected and its electromagnetic problem was formulated for a single layer of coating using a homogeneous material with arbitrary permittivity or permeability parameters. It was shown that with a constant slot excitation, the radiated power was enhanced at mode resonances.

Ever since the turn of the millennium, there had been an explosive growth in the amounts of research invested into the area of metamaterials or left-handed materials. This classifies artificially synthesized materials with negative permittivity and/or permeability over a finite frequency band. When both the permittivity and permeability are simultaneously negative, they are known as double negative (DNG) materials. There had been many claimed applications of metamaterials, with interesting and novel results, among which are the mode resonances in layered structures as well as in obtaining electrically small and efficient antennas, waveguide miniaturization, reducing the peak SAR in the human head, amongst others. Specific applications involving the coating of radiators and scatterers with metamaterial layers are in the enhancement of the radiation efficiency [6] and directivity [7, 8], as well as the reduction of

sidelobes [8]. There had also been studies of anomalous scattering by conducting cylinders coated with metamaterials [9]. Works associated with the studies of unusual resonances caused by metamaterials [10] for achieving improved efficiencies [11], strong field localization [12], and even microwave filtering in waveguides [13] were also conducted. Other interesting applications have also been considered and studied, and a good summary of them can be viewed in recent manuscripts [14–16]. Such new concepts of unnatural but novel materials with negative parameters motivate a rejuvenation of research into coated spherical antennas, but this time, with coverings composed of metamaterials.

The shortcoming of the investigations in [5] is in neglecting to relate the output parameters of the antennas like the radiated power and directivity to its input power, in order to satisfy the law of energy conservation. This study is undertaken to close this gap and develop expressions consistent with conservation laws and useable in practical antenna designs. The case of slotted conducting spherical antenna is selected again, as it allows developing exact expressions for the field equations, and determination of their solutions. To include the effects of metamaterials on the resonances, the case of double layer coating, as opposed to a single layer coating in [5], is now considered. A schematic of this structure is provided in Fig. 1. The purpose of studying two layers is to explore the combined effects of a natural and metamaterial coating. The additional degrees of freedom provided by the second layer open up to a range of aspects for investigations which is not available in single-coated spheres. It also allows the correct interpretation of excessive power radiation from constant current or

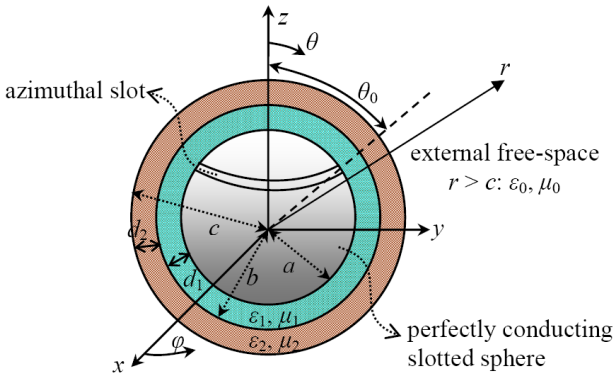

Figure 1. Schematic of perfectly conducting sphere with a narrow azimuthal excitation slot, and coated with two layers of homogeneous materials.

voltage sources involving mode resonances in metamaterials, thus resolving the related power paradox.

Therefore, the objectives of this paper are to detect the coating resonances and study their influences on the antenna radiated power and directivity. They are then related to the input power and the consequences of the coating resonances are discussed. This paper shall investigate the use of materials with negative constitutive parameters as the coatings of azimuthally-slotted metallic spheres. Exact formulations are developed herein. Primary aspects to be focused upon are the resonance effects brought about by the metamaterial coatings, and their corresponding comparisons with ordinary coat materials. Radiation patterns will also be looked into. The selected geometry of a slotted sphere is a form of dipole antenna, and its study represents a practical problem in antennas radiating in the presence of materials and metamaterials, helping to resolve the causes of unusual radiation characteristics.

2. ANALYSIS AND FORMULATION

Figure 1 shows a perfectly conducting sphere of radius a, with a narrow azimuthal slot located at $\theta = \theta_0$, and coated with two layers of homogeneous materials, such that the radii up to the first and second coatings are b and c, respectively. The inner and outer coatings are labeled by indices 1 and 2, respectively, with corresponding parameters: ε_1, μ_1, and ε_2, μ_2, as shown in the figure. The analysis that follows is based on the classical method of vector potentials [17, 18].

2.1. Field Expressions in Layers via Vector Potentials

The thin slot gives rise to the following excitation electric field which exists only over the slot.

$$E_\theta^{slot}\Big|_{\substack{r=a,\\ \theta=\theta_0}} = E_0\delta\left(\theta-\theta_0\right), \quad E_\phi \equiv 0 \tag{1}$$

where E_0 is an arbitrary amplitude coefficient and δ the Dirac delta function. Due to the purely azimuthal radiated magnetic field from this azimuthal slot, the dominant mode of the radiated field is TM^r. This dictates the following radial components of the electric (F) and magnetic (A) vector potentials.

$$F_r^{(1)} \equiv F_r^{(2)} \equiv 0, \quad A_r^{(1)} \neq 0, \quad A_r^{(2)} \neq 0 \tag{2}$$

where the bracketed superscript denotes the layer index: (1) for the inner layer $a \leq r \leq b$ and (2) for the outer layer $b \leq r \leq c$. Assuming

only the zeroth-order variation along the azimuthal direction, i.e., no variation along φ,

$$\frac{\partial A_r^{(i)}}{\partial \phi} = 0 \tag{3}$$

in which the bracketed superscript (i) may represent either (1) or (2) for the inner or outer coating layers, respectively, or (0) for the external free-space. The radial components of the magnetic vector potentials within the inner ($a < r < b$) and outer ($b < r < c$) dielectric coating layers, and the external free-space region ($r > c$) outside the sphere are written as

$$A_r^{(1)} = \sum_{n=1}^{\infty} \left[a_n^{(1)} \hat{J}_n(k_1 r) + b_n^{(1)} \hat{Y}_n(k_1 r) \right] P_n^{m=0}(\cos\theta) \tag{4a}$$

$$A_r^{(2)} = \sum_{n=1}^{\infty} \left[a_n^{(2)} \hat{J}_n(k_2 r) + b_n^{(2)} \hat{Y}_n(k_2 r) \right] P_n^{m=0}(\cos\theta) \tag{4b}$$

$$A_r^{(0)} = \sum_{n=1}^{\infty} c_n \hat{H}_n^{(2)}(k_0 r) P_n^{m=0}(\cos\theta) \tag{4c}$$

where $\hat{J}$ and $\hat{Y}$ are the well-known Riccati or Schelkunoff type spherical Bessel functions [17], and $P_n^m(\cos\theta)$ is the nth order associated Legendre function with the characteristic index m. These Riccati functions are related to the more common Bessel functions via the following.

$$\hat{K}_n(kr) = \sqrt{\frac{\pi kr}{2}} K_{n+1/2}(kr) \tag{4d}$$

where K may be either J, Y, or $H_n^{(2)}$ [11]. The five amplitude coefficients: $a_n^{(1)}$, $b_n^{(1)}$, $a_n^{(2)}$, $b_n^{(2)}$, and c_n, are so far unknown and are to be determined.

Using the following well-known expressions of the electric and magnetic field components in terms of the vector potential [18],

$$E_\theta = \frac{1}{j\omega\mu\varepsilon r} \frac{\partial^2 A_r}{\partial r \partial \theta}, \qquad H_\phi = -\frac{1}{\mu r} \frac{\partial A_r}{\partial \theta} \tag{5}$$

these field components in the various layers are stated as follow.

$$E_\theta^{(1)} = \frac{1}{j\sqrt{\mu_1 \varepsilon_1} r} \sum_{n=1}^{\infty} \left[a_n^{(1)} \hat{J}_n'(k_1 r) + b_n^{(1)} \hat{Y}_n'(k_1 r) \right] P_n^1(\cos\theta) \tag{6a}$$

$$E_\theta^{(2)} = \frac{1}{j\sqrt{\mu_2 \varepsilon_2} r} \sum_{n=1}^{\infty} \left[a_n^{(2)} \hat{J}_n'(k_2 r) + b_n^{(2)} \hat{Y}_n'(k_2 r) \right] P_n^1(\cos\theta) \tag{6b}$$

$$E_\theta^{(0)} = \frac{1}{j\sqrt{\mu_0\varepsilon_0}r}\sum_{n=1}^{\infty} c_n \hat{H}_n^{(2)'}(k_0 r) P_n^1(\cos\theta) \tag{6c}$$

$$H_\phi^{(1)} = -\frac{1}{\mu_1 r}\sum_{n=1}^{\infty}\left[a_n^{(1)}\hat{J}_n(k_1 r) + b_n^{(1)}\hat{Y}_n(k_1 r)\right] P_n^1(\cos\theta) \tag{6d}$$

$$H_\phi^{(2)} = -\frac{1}{\mu_2 r}\sum_{n=1}^{\infty}\left[a_n^{(2)}\hat{J}_n(k_2 r) + b_n^{(2)}\hat{Y}_n(k_2 r)\right] P_n^1(\cos\theta) \tag{6e}$$

$$H_\phi^{(0)} = -\frac{1}{\mu_0 r}\sum_{n=1}^{\infty} c_n \hat{H}_n^{(2)}(k_0 r) P_n^1(\cos\theta) \tag{6f}$$

whereby the following identity has been used in obtaining the above equations.

$$\sin\theta \frac{dP_n^{m=0}(\cos\theta)}{d(\cos\theta)} = -P_n^{m=1}(\cos\theta) \tag{7}$$

Before proceeding, the following orthogonality property useful to the forthcoming formulation is first stated.

$$\int_{\theta=0}^{\pi} P_n^1(\cos\theta) P_q^1(\cos\theta)\sin\theta d\theta = \begin{cases} 0, & q \neq n \\ \frac{2n(n+1)}{2n+1}, & q = n \end{cases} \tag{8}$$

2.2. Boundary Conditions

The boundary conditions to be imposed require the continuity of the tangential fields across the boundaries separating the various layers, namely at $r = a$, $r = b$, and $r = c$.

Upon enforcing the continuities of the tangential θ-components of the electric field across the three interfaces $r = a$, $r = b$ and $r = c$, the following are acquired.

$$\frac{\sum_{n=1}^{\infty}\left[a_n^{(1)}\hat{J}_n'(k_1 a) + b_n^{(1)}\hat{Y}_n'(k_1 a)\right] P_n^1(\cos\theta)}{ja\sqrt{\mu_1\varepsilon_1}} = E_0\delta(\theta - \theta_0) \tag{9a}$$

$$\begin{aligned}&\sqrt{\mu_2\varepsilon_2}\sum_{n=1}^{\infty}\left[a_n^{(1)}\hat{J}_n'(k_1 b) + b_n^{(1)}\hat{Y}_n'(k_1 b)\right] P_n^1(\cos\theta) \\ =\ &\sqrt{\mu_1\varepsilon_1}\sum_{n=1}^{\infty}\left[a_n^{(2)}\hat{J}_n'(k_2 b) + b_n^{(2)}\hat{Y}_n'(k_2 b)\right] P_n^1(\cos\theta)\end{aligned} \tag{9b}$$

$$\sqrt{\mu_0\varepsilon_0}\sum_{n=1}^{\infty}\left[a_n^{(2)}\hat{J}_n'(k_2c)+b_n^{(2)}\hat{Y}_n'(k_2c)\right]P_n^1(\cos\theta)$$
$$=\sqrt{\mu_2\varepsilon_2}\sum_{n=1}^{\infty}c_n\hat{H}_n^{(2)'}(k_0c)P_n^1(\cos\theta) \tag{9c}$$

Making use of the orthogonality property of (8), we obtain

$$a_n^{(1)}\hat{J}_n'(k_1a)+b_n^{(1)}\hat{Y}_n'(k_1a)=\frac{jE_0a\sqrt{\mu_1\varepsilon_1}\,(2n+1)}{2n\,(n+1)}P_n^1(\cos\theta_0)\sin\theta_0 \tag{10a}$$

$$a_n^{(1)}\hat{J}_n'(k_1b)+b_n^{(1)}\hat{Y}_n'(k_1b)-\sqrt{\frac{\mu_1\varepsilon_1}{\mu_2\varepsilon_2}}\left[a_n^{(2)}\hat{J}_n'(k_2b)+b_n^{(2)}\hat{Y}_n'(k_2b)\right]=0 \tag{10b}$$

$$a_n^{(2)}\hat{J}_n'(k_2c)+b_n^{(2)}\hat{Y}_n'(k_2c)-\sqrt{\frac{\mu_2\varepsilon_2}{\mu_0\varepsilon_0}}c_n\hat{H}_n^{(2)'}(k_0c)=0 \tag{10c}$$

The continuities of the tangential φ-components of the magnetic field across $r=b$ and $r=c$ are stated as

$$\frac{1}{\mu_1}\sum_{n=1}^{\infty}\left[a_n^{(1)}\hat{J}_n(k_1b)+b_n^{(1)}\hat{Y}_n(k_1b)\right]P_n^1(\cos\theta)$$
$$=\frac{1}{\mu_2}\sum_{n=1}^{\infty}\left[a_n^{(2)}\hat{J}_n(k_2b)+b_n^{(2)}\hat{Y}_n(k_2b)\right]P_n^1(\cos\theta) \tag{11a}$$
$$\frac{1}{\mu_2}\sum_{n=1}^{\infty}\left[a_n^{(2)}\hat{J}_n(k_2c)+b_n^{(2)}\hat{Y}_n(k_2c)\right]P_n^1(\cos\theta)$$
$$=\frac{1}{\mu_0}\sum_{n=1}^{\infty}c_n\hat{H}_n^{(2)}(k_0c)P_n^1(\cos\theta) \tag{11b}$$

Applying the same orthogonality property of (8) again, (11a) and (11b) give

$$\mu_2\left[a_n^{(1)}\hat{J}_n(k_1b)+b_n^{(1)}\hat{Y}_n(k_1b)\right]-\mu_1\left[a_n^{(2)}\hat{J}_n(k_2b)+b_n^{(2)}\hat{Y}_n(k_2b)\right]=0 \tag{12a}$$

$$\mu_0\left[a_n^{(2)}\hat{J}_n(k_2c)+b_n^{(2)}\hat{Y}_n(k_2c)\right]-\mu_2c_n\hat{H}_n^{(2)}(k_0c)=0 \tag{12b}$$

Equations (10a), (10b), (10c), (12a), and (12b) constitute the five equations in terms of the five unknowns: $a_n^{(1)}$, $b_n^{(1)}$, $a_n^{(2)}$, $b_n^{(2)}$, and c_n, which can then be solved for. This linear system of equations may be cast in matrix form:

$$[Z]_{5\times5}\,[C]_{5\times1}=[F]_{5\times1};\;\; [C]_{5\times1}=\left[\begin{array}{ccccc} a_n^{(1)} & b_n^{(1)} & a_n^{(2)} & b_n^{(2)} & c_n \end{array}\right]^{\mathrm{T}}$$
$$[F]_{5\times1}=\left[\frac{jE_0a\sqrt{\mu_1\varepsilon_1}(2n+1)}{2n(n+1)}P_n^1(\cos\theta_0)\sin\theta_0 \quad 0 \;\; 0 \;\; 0 \;\; 0\right]^{\mathrm{T}} \tag{13a}$$

where the latter column vector represents the driving force. By Cramer's rule, the solution of each coefficient involves a division by the determinant of the coefficient matrix $[Z]$ (the quotient). The divisor is also the determinant of a matrix, say $[D]$, which is just $[Z]$ but with one of its columns replaced by $[F]$. Note that E_0 does not occur in $[Z]$. The general form of the coefficient may be expressed as

$$\alpha = |D_\alpha|/|Z| \tag{13b}$$

where α may be any one of the five amplitude coefficients. The subscript α of D is to signify that there is one particular matrix D for each α. The coefficient matrix $[Z]$ is written as

$$[Z] = \begin{bmatrix} \hat{J}'_n(k_1a) & \hat{Y}'_n(k_1a) & 0 & 0 \\ \hat{J}'_n(k_1b) & \hat{Y}'_n(k_1b) & -\sqrt{\frac{\mu_1\varepsilon_1}{\mu_2\varepsilon_2}}\hat{J}'_n(k_2b) & -\sqrt{\frac{\mu_1\varepsilon_1}{\mu_2\varepsilon_2}}\hat{Y}'_n(k_2b) \\ 0 & 0 & \hat{J}'_n(k_2c) & \hat{Y}'_n(k_2c) \\ \mu_2\hat{J}_n(k_1b) & \mu_2\hat{Y}_n(k_1b) & -\mu_1\hat{J}_n(k_2b) & -\mu_1\hat{Y}_n(k_2b) \\ 0 & 0 & \mu_0\hat{J}_n(k_2c) & \mu_0\hat{Y}_n(k_2c) \end{bmatrix}$$

$$\begin{bmatrix} 0 \\ 0 \\ -\sqrt{\frac{\mu_2\varepsilon_2}{\mu_0\varepsilon_0}}\hat{H}_n^{(2)'}(k_0c) \\ 0 \\ -\mu_2\hat{H}_n^{(2)}(k_0c) \end{bmatrix} \tag{14}$$

The 5×1 excitation matrix $[F]$ has only one non-zero term located at the first element node, which is given by the right hand side of (10a). Therefore, a solution exists as long as the determinant of the matrix (14) is non-zero, or it does not become ill-conditioned. Either of these cases corresponds to the resonance of modes in the coating, and the solution of the matrix Equation (13a) fails. Or, the computed coefficients for one of the modes become exceptionally larger than the others, indicating a partial resonance of modes inside the coating. Enforcing the causality conditions and conservation of energy, the effects of such resonances on the antenna radiated power and directivity are discussed later, allowing a meaningful resolution to the uncertainties caused by these resonances.

2.3. Radiated Power

Using the well-known Poynting vector of the radiated field, the radiated power is

$$P_{rad} = \frac{r^2}{2}\mathrm{Re}\int_{\phi=0}^{2\pi}\int_{\theta=0}^{\pi} E_\theta^{(0)} H_\phi^{(0)*} \sin\theta d\theta d\phi \tag{15a}$$

Applying (6c) and (6f) in this equation and using the orthogonality property of (8) as well as the asymptotic forms of the Hankel functions for large arguments, the radiated power is simplified to

$$P_{rad} = \frac{2\pi}{\mu_0\sqrt{\mu_0\varepsilon_0}} \sum_{n=1}^{\infty} |c_n|^2 \frac{n\,(n+1)}{2n+1} \tag{15b}$$

Naturally, the radiated power depends on the mode coefficients c_n of the external free space region, which as mentioned earlier, involve a division by the matrix determinant in (14).

2.4. Directive Gain Patterns

The well-known expression of the directive gain function is [19]

$$D_0(\theta,\phi) = 4\pi U(\theta,\phi)/P_{rad} \tag{16}$$

where $U(\theta,\phi)$ is the radiation intensity given in this case [19]

$$U(\theta,\phi) = r^2\Big(|E_\theta(\theta,\phi)|^2 + |E_\phi(\theta,\phi)|^2\Big)\Big/2\eta \tag{17}$$

Thus, using the results from (6c), (6f), and (15b) the antenna directive gain becomes

$$D_0(\theta) = \frac{\left|\sum\limits_{n=1}^{\infty} c_n P_n^1(\cos\theta) e^{jn\pi/2}\right|^2}{\sum\limits_{n=1}^{\infty} |c_n|^2 \frac{n(n+1)}{2n+1}} \tag{18}$$

Note that, if the antenna conductor and the layered media are all lossless, the above directive gain becomes the antenna directivity. The knowledge of the coefficients c_n, computed using the above mentioned procedure, provides the directive gain plots, from which one can also determine the antenna peak directivity.

3. NUMERICAL RESULTS AND DISCUSSIONS

In this section, we present the computed radiated power, as presented in (15b). Under modal resonances, the matrix determinant $|Z|$ vanishes and results in explosive growth of the mode coefficients contained in solution vector $[C]$ of (13a), as mentioned earlier. Thus in using (15b), the computed radiated power will show peaks at mode resonances.

To verify the above properties, two groups of investigations into the radiation of a doubly-coated sphere are conducted. In the first group, the thicknesses of the inner and outer coatings are changed, and in the second the material properties of one layer and the thickness of

the other layer are modified. For all computed results to come, the radius a of the metal sphere is such that $k_0a = 1$, and an equatorial slot is treated, i.e., $\theta_0 = \pi/2$. The sphere size $k_0a = 1$ without coating is a useful size to study. Larger sphere sizes provide more resonant modes, but the results will follow similar trends.

3.1. Thickness Variation of Both Coatings

Various combinations of the permittivities of the two coating layers are investigated, and the results for 12 representative cases are provided. Specifically, two relative permittivities of 4 and 9 and their negative values are considered. In the first ten cases the relative permeability of both regions is positive and unity ($\mu_r = 1$). The permittivity combination pairs are: $(+4, +4)$, $(+9, +9)$, $(+4, +9)$, $(+9, +4)$, $(-4, -9)$, $(-9, -4)$, $(+4, -9)$, $(+9, -4)$, $(-4, +9)$, $(-9, +4)$, where the relative permittivity of the inner layer is stated first in each parenthesis. In these cases, the negative permittivity will cause evanescent fields in that region. The last two cases have a negative permeability ($\mu_r = -1$) for both layers and negative permittivities of $(-4, -9)$ and $(-9, -4)$. Thus, the fields are again of propagating types in the two coating regions.

Before proceeding further, let us just take a short moment to speak of the physical ramifications of materials with oppositely-signed or doubly-negative parameters. For the case of positive permeability but negative permittivity, we have the so-called ENG (epsilon negative) materials, whereas when the permittivity is positive but the permeability is negative, we have MNG (mu negative) materials. And when both the permittivity and permeability are negative, we have DNG (double negative) materials, also known as metamaterials. Needless to say then, for the usual materials with positive permittivity and positive permeability, they are termed as DPS (double positive). Both ENG and MNG properties can individually be exhibited by naturally-existing materials within specific frequency bands without human intervention. In certain frequency regimes, many plasmas exude negative permittivities in conjunction with positive permittivities, i.e., ENG materials. For instance, noble metals (e.g., gold, silver) behave in this manner in the infrared and visible spectrum. Whereas, MNG characteristics are physically displayed by gyromagnetic materials. However, only DNG materials cannot be found in nature, thus their alternative name "metamaterials", suggestive of paranormal properties beyond those of natural substances. Nonetheless, they (DNG) as well as ENG and MNG materials can all be artificially synthesized, particular even at frequencies other than those of naturally-occurring matter. The most common way to mimic ENG materials is

by a periodic array of parallel thin metallic wires, whereas the straightforward method to artificially construct MNG materials is by a likewise regular lattice of capacitively-loaded metallic loops (typically split ring resonators, or SRR). By straightforward combination of both constructs, a DNG metamaterial can be artificially fabricated as a composite of the thin-wire array ENG structure and the split-ring array MNG, exhibiting a macroscopic permittivity and permeability which are at least close to that of the wire-array ENG and SRR-lattice MNG medium, respectively, albeit being a simplified model that neglects interactions between the wires and rings. In all three frameworks, the period (inter-element spacing) must be considerably less than the wavelength in order for a homogenization effect to take place.

Nevertheless, while naturally-occurring ENG and MNG properties can be prevalent over a rather broad range in the frequency spectrum, artificially synthesized ENG, MNG and DNG attributes are generally if not mostly narrow-banded. Arguably, the most common way to mathematically express the frequency dependency of the permittivity and permeability of ENG and MNG materials is derived by the Drude model [14]:

$$\varepsilon(f) = \varepsilon_0 \left[1 - \frac{f_{p_e}^2}{f\left(f - j\frac{\Gamma_e}{2\pi}\right)}\right]$$

$$\mu(f) = \mu_0 \left[1 - \frac{f_{p_m}^2 - f_{0_m}^2}{f^2 - f_{0_m}^2 - j\frac{\Gamma_m f}{2\pi}}\right]$$

where ω_{p_e} and Γ_e are respectively the plasma and damping frequencies for ENG materials, and correspondingly ω_{p_m} and Γ_m for MNG materials. These damping factors constitute losses. In a lossless system, the Γ terms vanish and by mere inspection, both the permittivity and permeability are positive when the frequency is above the plasma frequency, but are negative when the frequency is less than the plasma frequency, with resultant imaginary refractive indices. Consequently, the only solutions are evanescent waves, which are still physically realistic phenomena.

As seen from (15b), P_{rad} is a combined sum of an infinite number of modal powers. In reality, this summation has to be truncated to a finite number of modal powers. Fortunately, the powers carried by higher order modes (with n larger than $k_0 a = 1$) decrease rapidly, and their contribution to the radiated power becomes negligibly small as compared to the fundamental (lower order) modes. Moreover, for the present symmetric excitation $\theta_0 = \pi/2$, the powers carried by modes of even n are zero. Hence, only odd modal indices n need to be considered in the summation. In the upcoming computed results,

we have truncated to the first 4 odd modes, i.e., for $n = 1$ to 7. In addition, a fixed $E_0 = 1$ of (1) has been maintained throughout the computations.

Figure 2 presents three-dimensional plots of P_{rad} as a function of the coating thicknesses $d(\lambda_j)$ of the two layers (normalized to their respective absolute dielectric wavelengths: $|\lambda_j| = |1/[f\sqrt{(\mu_j \varepsilon_j)}]|$, where j is 1 or 2, and f is the frequency) for various combinations of inner and outer relative permittivities, all with absolute values of 4 and 9 (those stated earlier in parentheses). The normalized coating thicknesses range from 0 to 1 for both layers. As can be seen, there are distinct peaks in the plots of P_{rad} and their locations and magnitudes are dependent on the selected coatings. The modes that cause the resonances are indicated in the plots. A brief explanation of the results is provided below.

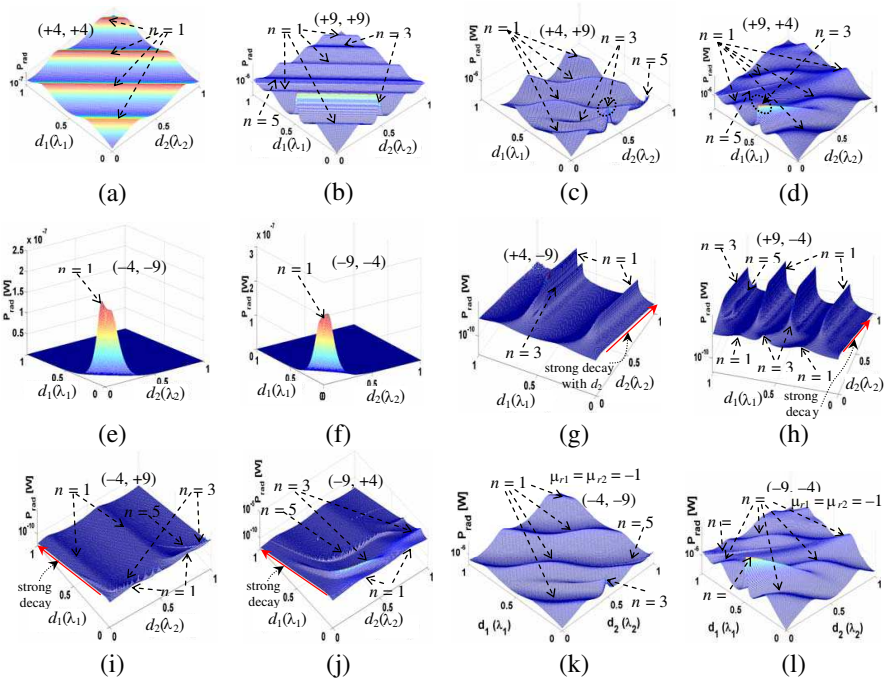

Figure 2. Total radiated power over various coating thicknesses of the two layers, for various combination pairs of relative permittivities as indicated in parentheses $(\varepsilon_{r1}, \varepsilon_{r2})$. The thicknesses d_1 and d_2 normalized to the respective **absolute** dielectric wavelengths $|\lambda_j| = |1/[f\sqrt{(\mu_j \varepsilon_j)}]|$ of the coating material range from 0 to 1. Cases (a) to (j) have $\mu_{r1} = \mu_{r2} = +1$, cases (k) and (l) have $\mu_{r1} = \mu_{r2} = -1$.

Figures 2(a) to 2(d) show the results when both coating permittivities are positive. Figs. 2(a) and 2(b) are for the case where both layers are identical: $(+4, +4)$ and $(+9, +9)$. Evidently, the profiles of these two contour plots are uniform along the diagonal paths, over which the total coating thickness is constant, and correspond to the singly-coated structures discussed in [5]. It is shown here as the reference case, and to indicate the number and location of the resonant modes.

The results for positive, but different, permittivities of the two layers, are provided in Figs. 2(c) and 2(d). The resonances are more complex in shape and intensity, and are mostly diffused. Two sharp resonances are indicated by two small circles around them.

When both coating permittivities are negative, the associated power profiles are given by Figs. 2(e) and 2(f). In this case, the modes are evanescent in both layers, in virtue of the imaginary negative refractive index as explained earlier, and power can reach the outermost region only if both coating thicknesses are small. The results clearly show this phenomenon, as the computed radiated powers are significant only near the bottom corner, where both coating thicknesses go to zero.

In Figs. 2(g) and 2(h), the permittivity of the inner coating is positive and that of the outer one is negative. This case is similar to the problem of the ionosphere, and the resonant modes correspond to Whispering Gallery Modes (WGM) [20]. Thus, the main parameter of importance is the thickness of the first layer, which decides on the mode resonances. Hence, the computed peaks are clearly defined for certain thickness of the first coating layer. The second coating layer cannot support propagating modes, and the power penetration to the external region must decrease rapidly with its thickness. This is indeed shown in the figures, although it is not so obvious due to the logarithmic vertical scale, which makes the decay appear less severe than it really is. The radiated powers actually fall by as much as 50 dB from the maximum values at low thicknesses of the outer coating.

The next cases, when the permittivity of only the first layer is negative, are shown in Figs. 2(i) and 2(j). Here, the first layer supports the evanescent modes and the radiated power decreases with its thickness, as observed in the plots (again note the logarithmic vertical scale — hence the decay is actually much more rapid than it seems). However, the thickness of the second layer defines the resonances corresponding to this layer, and their presences are indicated by shallow wave-like form of the radiated power as a function of the second layer thickness. Interestingly, distinct and sharp resonant modes, attributed to the higher order $n = 3$ and $n = 5$, are also shown in

these two cases. Their locations seem dependent on the thicknesses of both coating layers.

As a final illustration of this study of coating thickness variation, two cases in which both layers are made of double-negative materials are presented in Figs. 2(k) and 2(l). The common relative permeability shared by the two coatings is -1. In this way, the modes within neither layer are evanescent. It is interesting to observe that the mode contours and the resonance intensities are the same as those in Figs. 2(a) and 2(b), for the double positive materials.

3.2. Material and Thickness Variations

For further investigations of the resonance effects, Figs. 3 and 4 are included, in which the material parameters of the inner layer (with a fixed thickness) and the thickness of the outer layer (with fixed

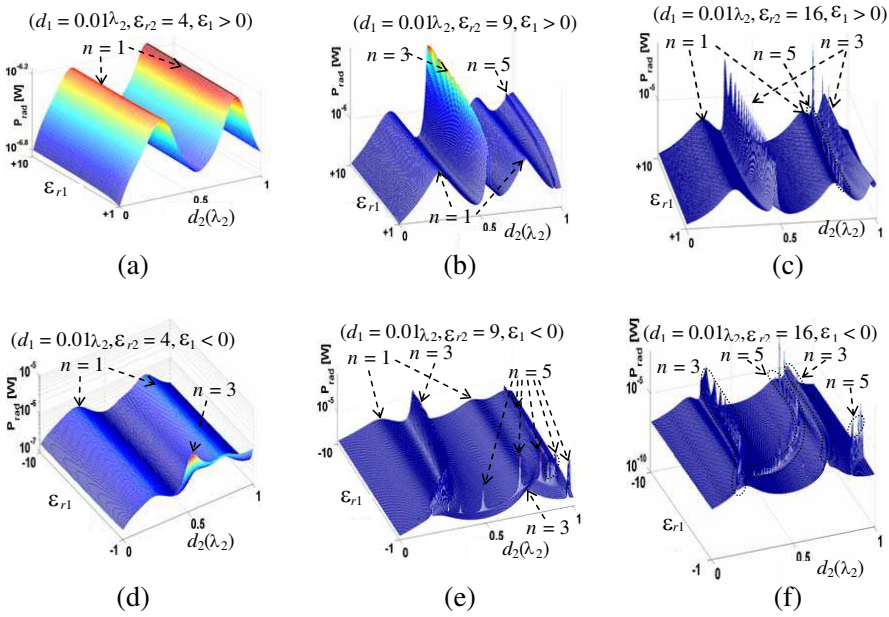

Figure 3. Total radiated power as a function of the permittivity ε_1 of the inner layer and thickness d_2 of the outer layer, for positive and negative ε_1, and various positive relative permittivities ε_{r2} of the outer layer (4, 9 and 16), as indicated. The outer coat thickness d_2 normalized to its dielectric wavelength $\lambda_2 = 1/[f\sqrt{(\mu_2\varepsilon_2)}]$ ranges from 0 to 1. **Inner coat thickness $d_1 = 0.01\lambda_2$.** Cases (a) to (c) are for $\varepsilon_1 > 0$, cases (d) to (f) are for $\varepsilon_1 < 0$. Relative permeability $\mu_{r1} = \mu_{r2} = 1$ throughout.

permittivity and permeability) are varied. The investigated thickness of the inner layer is small, being $0.01\lambda_2$. However in Fig. 3, the permeability of the inner layer is positive ($\mu_{r1} = 1$ throughout), but it is negative in Fig. 4 (and equal to its permittivity, i.e., $\varepsilon_1 = \mu_1 < 0$). The same spherical radius ($a = 1/k_0$) and equatorial slot ($\theta_0 = \pi/2$) of the previous subsection reapply. As before, the various modes contributing to the resonances are also indicated in the figures.

The plots of the total radiated power against the permittivity ε_1 of the inner layer and the thickness d_2 of the outer layer are given in Fig. 3, for positive and negative ε_1 values (Figs. 3(a) to 3(c) for the former, Figs. 3(d) to 3(f) for the latter). The fixed thickness of the inner layer, $d_1 = 0.01\lambda_2$ (see Fig. 1), is expressed in terms of the dielectric wavelength of the outer coating, $\lambda_2 = 1/f\sqrt{\mu_2\varepsilon_2}$ (f is the frequency), as indicated in each subplot of Fig. 3. The relative permittivity $\varepsilon_{r2} = \varepsilon_2/\varepsilon_0$ of the outer layer considered for each subplot

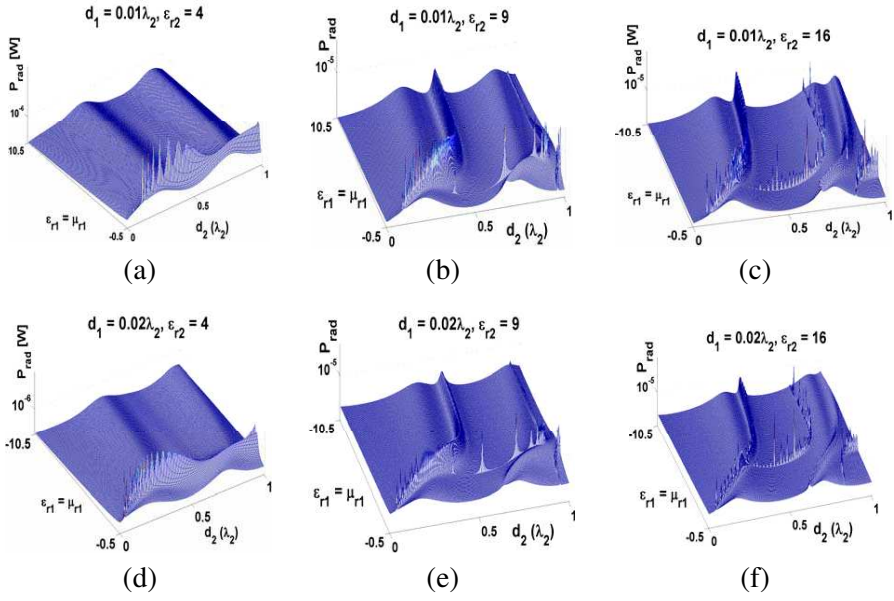

Figure 4. Total radiated power as a function of the **double negative parameter** ($\varepsilon_1 = \mu_1 < 0$) of the inner layer and thickness d_2 of the outer layer, for various relative permittivities ε_{r2} of the outer layer (4, 9, 16), as indicated. The outer coat thickness normalized to its dielectric wavelength $\lambda_2 = 1/[f\sqrt{(\mu_2\varepsilon_2)}]$ ranges from 0 to 1. **Inner coat thickness $d_1 = 0.01\lambda_2$ on the upper: cases (a) to (c), $d_1 = 0.02\lambda_2$ on the lower: cases (d) to (f).**

is also stated. The relative permittivity $\varepsilon_{r1} = \varepsilon_1/\varepsilon_0$ of the inner coating ranges from 1 to 10 for the positive values (left side plots of Fig. 3) and -1 to -10 for the negative ones (right side plots). As before, the normalized coating thickness of the outer layer ranges from 0 to 1. When the inner coating is composed of materials with negative permittivities, an evanescent region between the antenna and the outer layer with positive permittivity is created (remember that $\mu_{r1} = \mu_{r2} = 1$). Thus, for the right side plots of Fig. 3, the $n = 1$ mode resonances due to the thickness of the second layer are the same for all cases of inner coating permittivities. However, superimposed on these resonances are higher-order modal resonances attributed to the inner coating metamaterial, whose locations and intensities depend on the parameters of both layers. In particular, resonances occur for vanishing permittivity of the inner layer and vanishing thickness of the second layer. As such, inner coatings with negative permittivities are able to achieve resonances with outer coatings that are thinner than those attainable by ordinary inner coating materials. This will be demonstrated more clearly later. The attribution of the resonance peaks in these figures to various n-modes will be more distinctively specified in the upcoming Fig. 5.

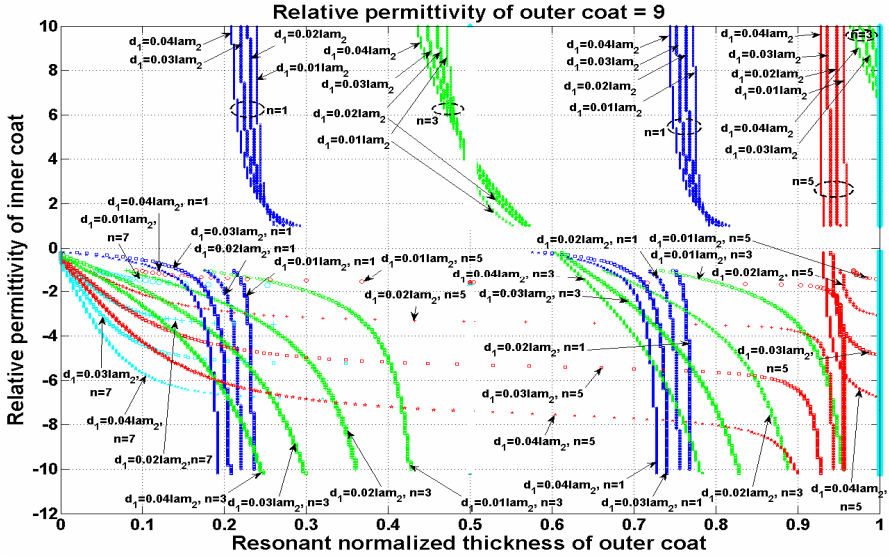

Figure 5. Contour paths of resonances extracted from Figs. 3(b) and 3(e), and several other d_1 cases ($0.02\lambda_2$, $0.03\lambda_2$, and $0.04\lambda_2$), for $\varepsilon_{r2} = 9$.

Figure 4 shows the same type of results as Fig. 3, but this time the simultaneously varied permittivity and permeability of the inner layer are equal and negative, i.e., $\varepsilon_1 = \mu_1 < 0$. Two different thicknesses $0.01\lambda_2$ and $0.02\lambda_2$ of the inner layer are investigated. It is interesting to note that the trends of the power profiles for this case are about the same as those in Fig. 3, which had a maintained $\mu_{r1} = 1$. This may be expected. However, it is important to present them here, as both regions are propagating and lossless. Thus, no power loss occurs and the radiated power becomes identical to the antenna input power (assuming it is matched to the source), a fact that is important for discussing the computed results and interpretation of the resonances.

The contour paths along which resonances occur in Fig. 3, as well as several more cases of thicker first layer ($d_1 = 0.02\lambda_2$, $0.03\lambda_2$, and $0.04\lambda_2$), are extracted and plotted in Fig. 5. In these graphs, the vertical axis represents the relative permittivity of the inner coating, whereas the resonant coating thickness of the outer layer constitutes the horizontal axis. As can be clearly seen from these plots, when the inner coatings possess small negative permittivities, the outer coating can be made very thin and still achieve resonances. On the other hand, such reductions in the resonant coating thickness of the outer layer cannot be achieved by inner coats made of ordinary materials with positive permittivities, regardless of their values. The

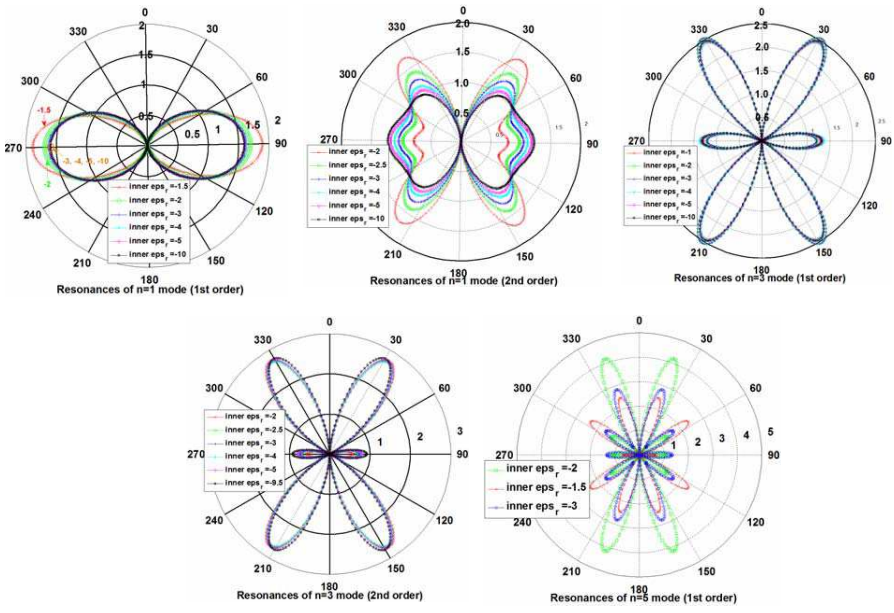

(a)

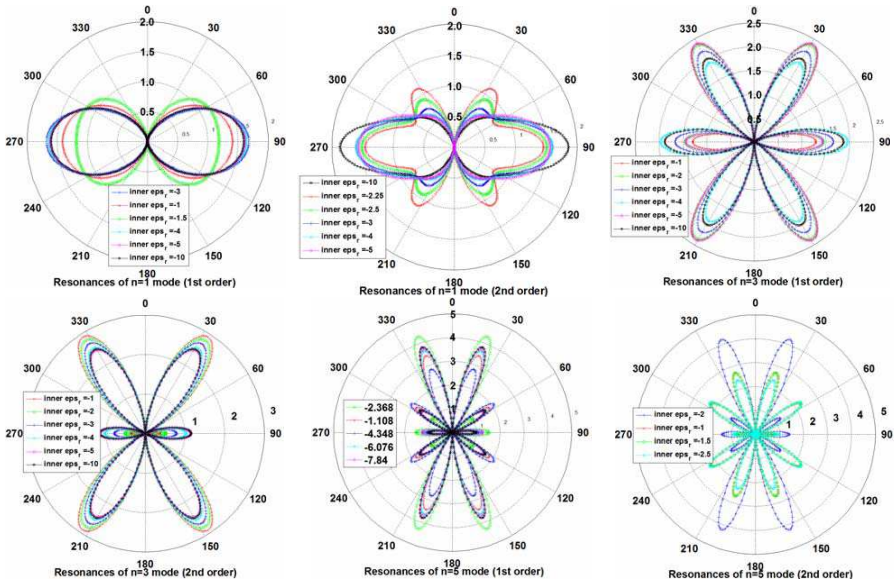

(b)

Figure 6. Directive gain patterns (variation with θ) generated by (18) for selected points along resonant paths of Fig. 5 (upper cluster) and an additional case of $\varepsilon_{r2} = +16$ (lower set), for $d_1 = 0.01\lambda_2$ and $\varepsilon_1 < 0$. Each cluster of plots corresponds to a certain ε_2, and each subplot within pertains to a certain nth mode. Relative permeability $\mu_{r1} = \mu_{r2} = 1$ throughout. (a) $\varepsilon_{r2} = +9$, $d_1 = 0.01\lambda_2$, $\varepsilon_1 < 0$ (of Fig. 5). (b) $\varepsilon_{r2} = +16$, $d_1 = 0.01\lambda_2$, $\varepsilon_1 < 0$.

key reason for this is the existence of resonance paths (see Fig. 3) introduced by the metamaterial, which swerve inwards towards the origin of the horizontal plane in the plots of Figs. 3(d) and 3(f), i.e., towards zero thickness of the outer coat. On the contrary, when the inner layer comprises natural materials, the resultant resonance paths either remain fairly unchanged with variations in the positive permittivity values, or swerve in the opposite direction, i.e., towards larger outer coat thicknesses instead. Hence, ordinary inner coat materials are unable to lower the profile of the outer layer and still maintain the resonance condition. Therefore, this marks an important attribute of coatings with negative permittivities, as such profile lowering in antenna technology at selected resonances offers dramatic improvements in miniaturized and even nanoscale antenna designs, which could not otherwise be feasible [14]. This strong radiation resonance for nearly zero coating thickness can be regarded as being related to nanofocusing [21–24], in which strong field localization

is achieved in the nanoscale, offering numerous modern applications such as imaging, spectroscopy, and optical ultra-microscopy, all with nanometer-scale spatial resolution, allowing even for single-molecule detection. It is also observed from Fig. 5 (as well as Fig. 3, but less obvious) that for sufficiently thin inner coatings ($d_1 = 0.01\lambda_2$ for our case), partial resonances (smooth humps) occur at about a common quarter wavelength thickness of the outer coating, regardless of the permittivity value of the inner layer. This quarter wavelength weak resonance is seen as the first smooth hump occurring at the lowest outer coat thickness in Fig. 3. Mild resonances also seem to appear at a common three-quarter wavelength thickness of the outer layer. Finally, the distinct modes causing the resonances of Fig. 3 are segregated out in Fig. 5, each being represented by a separate line.

For the inner coat thickness $d_1 = 0.01\lambda_2$, the directive gain patterns of arbitrarily selected points (each pertaining to a certain pair of ε_1 and d_2) along the resonant paths of Fig. 5 are plotted in Fig. 6, for $\varepsilon_1 < 0$. The rigorous form of (18) involving summation of modes has been used for generating these graphs. Each cluster of plots in this figure corresponds to a certain ε_2, and each subplot within the cluster pertains to a particular nth resonant mode, as clearly indicated. The parameter in each subplot is then ε_1. Due to the possible recurrences of resonances for any one mode (and ε_1) at multiple outer coat thicknesses, as seen in Fig. 5, orders of resonances for each nth mode are assigned. The first and second order resonances of some nth modes are separately plotted in Fig. 6. As can be observed, the radiation strengths towards any one direction for different ε_1 in each subplot do not vary appreciably from one another, with just notably varying levels along directions around the lobes. Moreover, a comparison between subplots of the same mode also shows only minor differences, i.e., fairly similar radiation patterns of the same nth mode amongst various outer coat permittivities ε_2. Hence, these suggest the independence of the directive gain of all parameters other than n and θ under resonance conditions.

It can also be seen that the number of lobes in the patterns (ranging from $\theta = 0$ to 180°) equals the mode index n. Recognizing this empowers one to configure a certain resonant pair of ε_1 and d_2 for achieving a prescribed radiation pattern with a desired gain and shaping the radiation patterns.

4. INTERPRETATION OF MODAL RESONANCES

Let the input power that is injected into the excited slot be P_{in}. From the theorem of power balance (or energy conservation), the

total radiated power P_{rad} expressed by (15b) plus the combined power lost through reflection (P_{refl}) as well as dissipation (P_{diss}) must then be equal to this P_{in}. Assuming a dissipation-less scenario (involving ideal lossless materials, i.e., $P_{diss} = 0$), the only avenue of power loss is via mismatch. Hence, the power conservation law can be stated mathematically as

$$P_{in} = P_{rad} + P_{refl} \tag{19}$$

With this laid, two scenarios may be considered: 1) non-resonance condition, and 2) resonance condition. The next paragraphs discuss these situations.

4.1. Resonant and Non-resonant Conditions

Under non-resonant conditions, the determinant $|Z|$ is finite and thus no one particular mode fully dominates over another. In this event, all terms in the series of (15b) and (18) are significant. However, for small sphere sizes, the magnitude of terms decreases with the order n, and the series converges rapidly, simplifying the computation.

The resonance condition, however, is significantly different. When the magnitude of $|Z|$ pertaining to a certain mode index n encounters a very small or zero value for a particular set of physical and electrical conditions, and assuming that this is the only resonant mode present, then all the other terms in the summation of (15b) may be dropped, since their contributions are overwhelmed by the solitary resonant term. Consequently, (19) may be restated with good approximation as

$$P_{rad}|_{n}^{reson} = \frac{2\pi}{\mu_0\sqrt{\mu_0\varepsilon_0}} |c_n|^2 \frac{n\,(n+1)}{2n+1} = P_{in} - P_{refl} \tag{20}$$

The power radiated by this nth mode then becomes seemingly very large, or infinite. However, by the conservation law, when the input power is finite a paradox is apparently at hand, and can be explained as follows. The mode coefficients of (4a) to (4c) may be written using (13b) as

$$\alpha = \frac{|D_\alpha|}{|Z|} = \left\{ \left[\frac{ja\sqrt{\mu_1\varepsilon_1}\,(2n+1)}{2n\,(n+1)} P_n^1(\cos\theta_0)\sin\theta_0 \right] |M_{1j}| \right\} \frac{E_0}{|Z|} \tag{21}$$

where $j = 1$ through 5 when α is $a_n^{(1)}$, $b_n^{(1)}$, $a_n^{(2)}$, $b_n^{(2)}$, and c_n, respectively, and $[M_{1j}]$ is the minor of $[Z]$ formed by eliminating the first row and the jth column of $[Z]$, thus being a 4×4 matrix. When $|Z| = 0$ under resonance, one can show from (14) the following relationship between the first two minors.

$$\hat{J}_n'(k_1a)\,|M_{11}| + \hat{Y}_n'(k_1a)\,|M_{12}| = 0 \tag{22}$$

Suppose initially that the trivial solution: $|M_{11}| = |M_{12}| = 0$ of this characteristic equation is admissible. Eq. (21) then says that $a_n^{(1)}$ and $b_n^{(1)}$ may still be finite (non-zero) if E_0 is also finite (non-zero). However, the condition of (22) says nothing about $|M_{15}|$, which thus certainly need not vanish, i.e., it is generally non-zero. Hence, if E_0 is non-vanishing, Eq. (21) dictates that c_n will become infinite when $|Z| = 0$. But such an infinite c_n cannot coexist with finite $a_n^{(1)}$ and $b_n^{(1)}$, due to violation of the boundary conditions as well as the power balance theorem (infinite power in the outermost region but finite power in the first layer). Therefore, the above trivial solution of (22) can only be valid if $E_0 = 0$. But in the most general case where this trivial solution is not permissible, i.e., all minor matrices are non-zero, then under resonance ($|Z| = 0$), a finite c_n is needed for a radiated power [see (15b)] that balances a finite fixed input power, P_{in}. As such, E_0 will also have to be zero, according to (21), so as to achieve a non-infinite c_n (a "zero divided by zero" situation). Hence, regardless trivial or nontrivial solutions of (22), E_0 has to vanish. Under such conditions, we arrive at the classical eigenvalue problem entailing the matrix equation: $[Z][C] = [0]$, for which non-trivial solutions exist only when $|Z| = 0$, which is the characteristic equation, as defined by (22). This means that non-vanishing field solutions exist (non-trivial eigenvector $[C]$) even without the presence of an excitation source ($E_0 = 0$), as of classical eigen-mode theory. For a certain fixed set of electrical and structural parameters, the eigenvalues then constitute the resonant eigen-modal frequencies which are solved for as roots of the characteristic equation $|Z| = 0$.

Therefore, returning to the diminishment of E_0 under resonance, contrary to what one may tend to expect when the power balance theorem is neglected, there is no infinite radiated power under modal resonance. Infinite radiation can only occur when there is an associated infinite source power. It is this conservation concept which addresses the resonance power paradox. However, it is reminded that in our present study, a constant E_0 has been considered, which corresponds to a constant (slot) voltage generator as opposed to a fixed power source. Hence, the radiated power profiles computed in Figs. 2 to 4 all pertain to different injected powers, instead of a constant input power shared amongst all structural configurations. This explains the varying "wavy" power profiles. Consequently, the radiated power can indeed take on infinite values under resonance conditions, although this entails a correspondingly infinite injected power (the conservation theorem), as said earlier. Had a constant power source been considered instead, and assuming zero mismatch losses, then the power profiles will all

take on the form of a uniform horizontal plane at the level of the input power.

Likewise, the directive gain of (18) under a resonance condition may be well approximated as

$$G_d|_{\substack{reson \\ n}} = \frac{(2n+1)\left|P_n^1(\cos\theta)\right|^2}{n\,(n+1)} \tag{23}$$

which is independent of the antenna and coating parameters. Hence, when a solitary nth mode is resonant, the directive gain is a function of only n and θ and is unaffected by other parameters of the structure. This is a remarkably interesting result. The physical and electrical properties of both the spherical antenna as well as the coatings no longer play a visible role in the antenna directivity. It is the resonating mode that decides on the antenna performance. Although of course, the antenna and coating parameters play an indirect role by exciting the resonant mode, but once the mode resonates, it decides on the radiation pattern and the antenna directivity. This property of the resonant modes is readily verified by recognizing that these calculated antenna radiation patterns near the resonant condition presented in Fig. 6 are highly similar to corresponding plots obtainable from (23).

A consequence of the above mode resonant property is the exact knowledge of the antenna directivity at mode resonances. For instance, for a symmetric excitation of the sphere with $\theta_0 = 90^\circ$, all even order ($n =$ even) associated Legendre functions vanish, and the terms in the series correspond to $n =$ odd integers. The directivity of the leading terms, in the horizontal $\theta = 90^\circ$ plane, can be shown to be,

$$n = 1,\ D_1(\theta = 90^\circ) = 1.50\ (1.76\,\text{dBi})$$
$$n = 3,\ D_3(\theta = 90^\circ) = 1.31\ (1.19\,\text{dBi})$$

The first term, for $n = 1$, corresponds to the dipole mode and its directivity of 1.5 is maximum in the horizontal plane. This is the same as that of an infinitesimal dipole. However, in the present case this directivity is obtained for all sphere and coating sizes and parameters, as long as the $n = 1$ mode resonates in the coating. For higher order modes, i.e., $n > 1$, the radiation patterns become more complex, given by $P_n^1(\cos\theta)$, and their peak directivities move away from the horizontal plane. Since these resonances are very sharp and generally narrow band, they can be used to design accurate gain standard probes for calibration of standard gain horns. Such probes can help in improving the accuracy of the gain measurement, which needs further investigation.

4.2. Apportionment of Total Radiated Power Amongst Modes

The apportionment of the total radiated power amongst the various modes for the gain patterns of the first, third, and fifth subplots in Fig. 6(b) for $n = 1$, 3, and 5 is conveyed in Figs. 7(a) to 7(c), respectively. As can be seen, under the conditions where the precision of resonance detection is high, i.e., strong modal power carried by

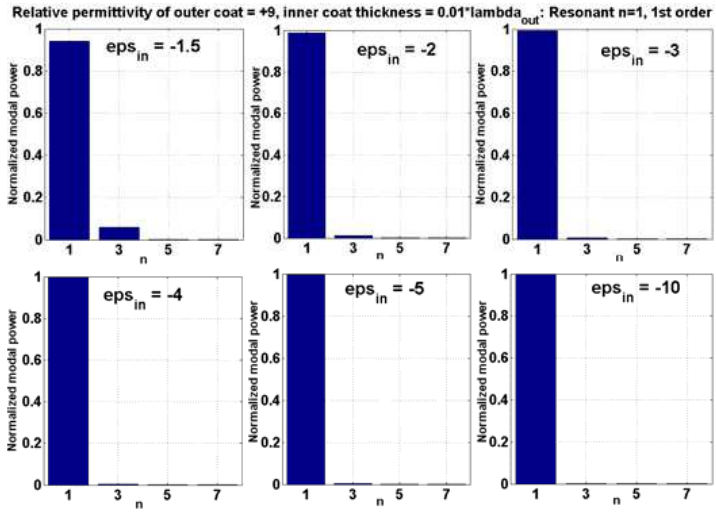

(a)

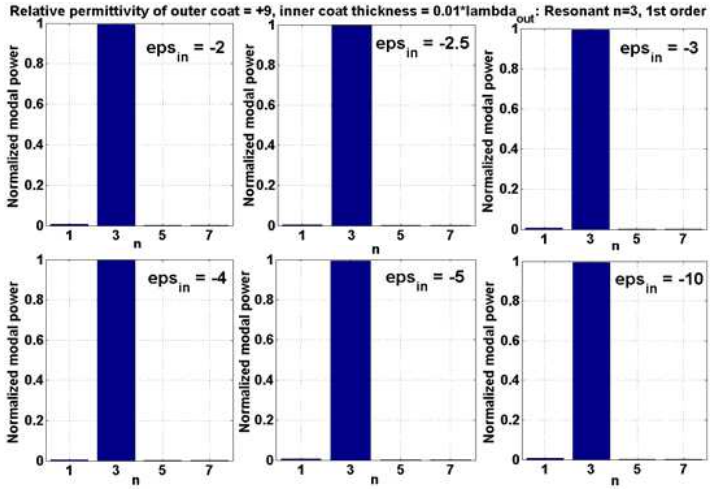

(b)

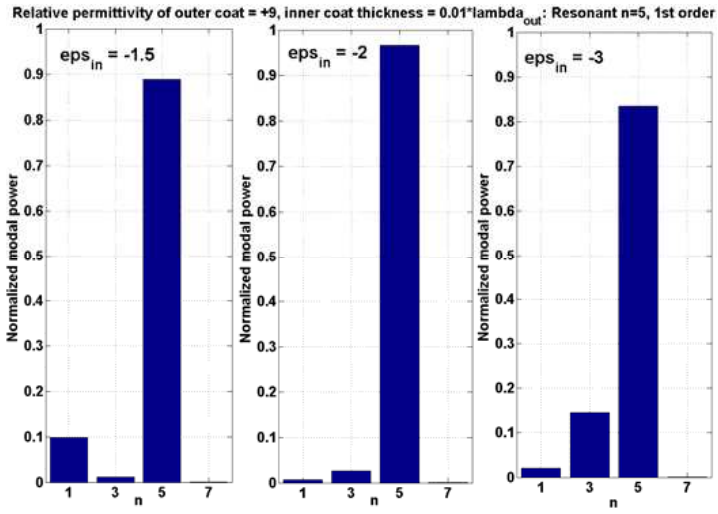

(c)

Figure 7. (a) Apportionment of modal powers amongst various n modes, for the same ε_1 cases as the **first subplot of Fig. 6(a) (resonant $n = 1$, 1st order**), with $\varepsilon_{r2} = +9$, $d_1 = 0.01\lambda_2$, $\varepsilon_1 < 0$. (b) Apportionment of modal powers amongst various n modes, for the same ε_1 cases as the **third subplot of Fig. 6(a) (resonant $n = 3$, 1st order)**, with $\varepsilon_{r2} = +9$, $d_1 = 0.01\lambda_2$, $\varepsilon_1 < 0$. (c) Apportionment of modal powers amongst various n modes, for the same ε_1 cases as the **fifth subplot of Fig. 6(a) (resonant $n = 5$, 1st order)**, with $\varepsilon_{r2} = +9$, $d_1 = 0.01\lambda_2$, $\varepsilon_1 < 0$.

the resonant mode as compared to the other non-resonant ones, the corresponding gain patterns of Fig. 6 are strongly identical to the idealized ones defined by (23).

5. CONCLUSIONS

The influence of coating materials on the radiation properties of a spherical dipole antenna was investigated. The excitation was assumed to be due to a circumferential slot, which made the antenna to resemble a thick dipole. The spherical geometry, however, allowed an exact analytical solution for the field equations and accurate determination of the antenna parameters like the radiated power and directivity. Formulations were developed for a double layer coating, to enable investigation of different coating types, especially with a combination of positive and negative parameters.

It was found that for coating materials with either only positive or only negative parameters, modes can resonate, provided the combined thickness of the two layers is at least around quarter dielectric wavelength. However, for materials with combined positive and negative parameters, the resonance can exist inside thinner coatings, the thickness of which can be made diminishingly small. It was also shown that with a constant slot excitation, the radiated power increases dramatically at mode resonances. However, under the scenario of a constant power generator, since the radiated power must be equal to the power of the source, the causality condition dictates that the slot excitation must reduce at resonances to maintain the radiated power at the level of the source power.

Another consequence of the mode excitation was to increase the contribution of the resonating mode to the radiated power, as compared to non-resonant modes. This fact was verified by calculating the radiated power of different contributing modes, which indicated that the radiation by non-resonant modes is negligible. The radiated field can then be expressed by the single resonating mode. This simplification permitted the exact calculation of the antenna directivity entirely by the resonating mode, which was also verified by the sample calculations. An important outcome of this resonance phenomenon was the fact that, at resonances, the antenna directivity became independent of the antenna size and coating size and physical parameters. It was decided entirely by the resonating mode. The constancy of the antenna gain at mode resonances, coupled with the simplicity of the antenna structure, allows the design of ultra-accurate gain standard probes for calibrating the Standard Gain Horns, commonly used for gain measurement. This will be a significant innovation in the area of antenna measurements.

ACKNOWLEDGMENT

The research for this work was supported by the National Science Council of Taiwan (NSC 100-2221-E-009-142 and NSC 101-2221-E-009-098).

REFERENCES

1. Karr, P. R., "Radiation properties of spherical antennas as a function of the location of the driving force," *J. Res. Natl. Bur. Stand.*, Vol. 46, 422–436, 1951.
2. Mushiake, Y. and R. E. Webster, "Radiation characteristics with

power gain for slots on a sphere," *IRE Trans. Antennas Propag.*, Vol. 5, No. 1, 47–55, Jan. 1957.

3. Kerker, M., *The Scattering of Light and Other Electromagnetic Radiation*, Academic Press, New York, 1969.
4. Towaij, S. J. and M. A. K. Hamid, "Diffraction by a multilayered dielectric-coated sphere with an azimuthal slot," *Proc. IEEE*, Vol. 119, 1209–1214, Sep. 1971.
5. Shafai, L. and R. K. Chugh, "Resonance effects in slotted spherical antennas coated with homogeneous materials," *Can. J. Phys.*, Vol. 51, 2341–2346, 1973.
6. Huang, M. D. and S. Y. Tan, "Efficient electrically small prolate spheroidal antennas coated with a shell of double-negative metamaterials," *Progress In Electromagnetics Research*, Vol. 82, 241–255, 2008.
7. Wu, B.-I., W. Wang, J. Pacheco, X. Chen, T. M. Grzegorczyk, and J. A. Kong, "A study of using metamaterials as antenna substrate to enhance gain," *Progress In Electromagnetics Research*, Vol. 51, 295–328, 2005.
8. Hamid, A. K., "Axially slotted antenna on a circular or elliptic cylinder coated with metamaterials," *Progress In Electromagnetics Research*, Vol. 51, 329–341, 2005.
9. Li, C. and Z. Shen, "Electromagnetic scattering by a conducting cylinder coated with metamaterials," *Progress In Electromagnetics Research*, Vol. 42, 91–105, 2003.
10. Brovenko, A., P. N. Melezhik, A. Y. Poyedinchuk, N. P. Yashina, and G. Granet, "Resonant scattering of electromagnetic wave by stripe grating backed with a layer of metamaterial," *Progress In Electromagnetics Research B*, Vol. 15, 423–441, 2009.
11. Choi, J. and C. Seo, "High-efficiency wireless energy transmission using magnetic resonance based on negative refractive index metamaterial," *Progress In Electromagnetics Research*, Vol. 106, 33–47, 2010.
12. Han, L., S. Chen, A. Schulzgen, Y. Zeng, F. Song, J.-G. Tian, and N. Peyghambarian, "Calculation and optimization of electromagnetic resonances and local intensity enhancements for plasmon metamaterials with sub-wavelength double-slots," *Progress In Electromagnetics Research*, Vol. 113, 161–177, 2011.
13. Siakavara, K. and C. Damianidis, "Microwave filtering in waveguides loaded with artificial single or double negative materials realized with dielectric spherical particles in resonance," *Progress In Electromagnetics Research*, Vol. 95, 103–120, 2009.

14. Engheta, N. and R. W. Ziolkowski, *Metamaterials Physics and Engineering Explorations*, IEEE Press, Wiley Interscience, New Jersey, 2006.
15. Eletheriades, G. V. and K. G. Balmain, *Negative-reflection Metamaterials, Fundamental Principles and Applications*, John Wiley and Sons Inc., New Jersey, 2005.
16. Caloz, C. and T. Ito, *Electromagnetic Metamaterials, Transmission Line, Theory and Microwave Applications*, John Wiley and Sons Inc., New Jersey, 2006.
17. Harrington, R. F., *Time-harmonic Electromagnetic Fields*, McGraw-Hill, New York, 1961.
18. Balanis, C. A., *Advanced Engineering Electromagnetics*, John Wiley and Sons, Inc., 1989.
19. Balanis, C. A., *Antenna Theory, Analysis and Design*, 3rd Edition, John Wiley and Sons Inc., New Jersey & Canada, 2005.
20. Budden, K. G. and H. G. Martin, "The ionosphere as a whispering gallery," *Proceedings of the Royal Soc. of London. Series A, Mathematical and Physical Sciences*, Vol. 265, No. 1323, 554–569, Feb. 1962.
21. Stockman, M. I., "Nanofocusing of optical energy in tapered plasmonic waveguides," *Physical Review Letters*, Vol. 93, No. 13, 2004, DOI: 10.1103/PhysRevLett.93.137404.
22. Seo, M. A., H. R. Park, S. M. Koo, D. J. Park, J. H. Kang, O. K. Suwal, S. S. Choi, P. C. M. Planken, G. S. Park, N. K. Park, Q. H. Park, and D. S. Kim, "Terahertz field enhancement by a metallic nano slit operating beyond the skin-depth limit," *Nature Photonics*, 152–156, 2009, DOI: 10.1038/NPHOTON.2009.22.
23. Sadiq, D., J. Shirdel, J. S. Lee, E. Selishcheva, N. Park, and C. Lienau, "Adiabatic nanofocusing scattering-type optical nanoscopy of individual gold nanoparticles," *Nano Letter*, Vol. 11, 1609–1613, 2011.
24. Kang, J. H., D. S. Kim, and Q. H. Park, "Local capacitor model for plasmonic electric field enhancement," *Physical Review Letter*, 1–2, 2010, DOI: 10.1103/PhyRevLett.102.093906.